Decorated-lattice model of metamagnetic or host-impurity systems*†

Carol K. Hall‡
Department of Physics, State University of New York, Stony Brook, New York 11790

George Stell
Department of Mechanics, State University of New York, Stony Brook, New York 11790

(Received 31 July 1973)

A study is made of the effect of adding a ferromagnetic interaction to Fisher's superexchange antiferromagnet. Our results can be considered as either the exact treatment for an infinitely weak and infinitely long-range ferromagnetic interaction or as the mean-field treatment for an arbitrary ferromagnetic interaction. In addition, our model is equivalent to a three-dimensional metamagnetic system in which spins in the same plane interact via a superexchange antiferromagnetic interaction while spins in different planes interact via a ferromagnetic interaction. When the model is interpreted as a host-impurity system, the results can be compared with those found experimentally for solutions of hydrogen in metals. We find that as the ratio of the antiferromagnetic to ferromagnetic coupling is varied, we reproduce qualitatively the behavior of the phase diagrams found when low and moderate concentrations of hydrogen are absorbed in palladium, in tantalum, and in niobium. Application of our model to absorption problems is also briefly discussed.

I. INTRODUCTION

It is of interest to find and study statistical models that are simple enough to permit an exact solution and yet are rich enough in structure to afford an insight into the relationship between the nature of the intermolecular potential and the phase-change behavior of the system. In this study we have considered a two-dimensional lattice model in a field whose intermolecular potential contains two terms: a reference term that represents a short-range antiferromagnetic interaction between spins and a perturbing term that is an infinitely weak and infinitely long-range ferromagnetic interaction between spins. The model can be solved exactly and yields a variety of phase-change behavior, which we describe in detail.

It can be shown[1,2] that the equation of state for a magnetic system with a two-body interaction potential that includes a reference term and an infinitely weak and infinitely long-range ferromagnetic perturbing term can be expressed in terms of the equation of state for the corresponding reference system (the potential of which contains only the reference term). This has enabled us to obtain the equation of state for our system, which has a short-range antiferromagnetic interaction and an infinitely weak and infinitely long-range ferromagnetic interaction, in terms of the equation of state for the reference system, which has only the short-range antiferromagnetic interaction.

Our reference system is Fisher's superexchange model,[3] which is a two-dimensional model of an antiferromagnet in which the antiferromagnetic coupling between magnetic Ising spins takes place indirectly. Magnetic spins are placed on the bonds of a lattice which contains a square array of nonmagnetic spins. This is called "decorating" the bond. These magnetic spins form a square array if viewed at an angle of 45° with respect to the original lattice. Each magnetic spin interacts with the two nonmagnetic spins at the ends of the bond, so that the interaction between magnetic spins is indirect. The superexchange model can be solved exactly in a field and exhibits behavior very much like that expected from the standard nearest-neighbor antiferromagnetic Ising model, which has yet to be solved exactly in a field.

The infinitely weak and infinitely long-range ferromagnetic interaction, which is the perturbing potential, may be characterized mathematically either as a limiting case of the equivalent-neighbor interaction,[1] which is given by $-(J/N)(\sum s_i)^2$ where J is finite and N is the total number of spins, or as a limiting case of the Kac potential,[2] which is given by $-J\gamma^d f(\gamma \vec{r}_{ij})$ where $\vec{r}_{ij}$ is the distance between particles i and j, d is the dimensionality, γ is a positive parameter, and $f(\gamma \vec{r}_{ij})$ is a positive function which satisfies certain weak conditions. In the thermodynamic limit of $N \to \infty$, the equivalent-neighbor potential becomes infinitely weak and infinitely long range. The Kac potential also becomes infinitely weak and infinitely long range in the limit of $\gamma \to 0$ after $N \to \infty$. Since these two potentials are identical after the limits are taken, we shall, for simplicity, give the discussion only in terms of the equivalent-neighbor potential. We wish to emphasize that our results can be viewed as either the exact treatment of an infinitely weak

and infinitely long-range potential or as a mean-field treatment of an arbitrary ferromagnetic interaction.[4]

Our model is also mathematically equivalent to a three-dimensional model of a metamagnet in which spins in the same plane interact via a superexchange antiferromagnetic interaction while spins in different planes interact via a ferromagnetic equivalent-neighbor interaction. Our treatment of the ferromagnetic interaction in this case may also be thought of as a mean-field treatment of an arbitrary ferromagnetic interaction.

Our model exhibits a variety of interesting behavior when it is interpreted as a host-impurity system. The phase diagrams are found to bear a striking qualitative resemblance to the phase diagrams found experimentally for several hydrogen-metal systems.[5] By varying the ratio of the anitferromagnetic to ferromagnetic coupling, the phase diagrams can be made to reproduce qualitatively the low- and moderate-concentration phase diagrams of hydrogen in palladium, hydrogen in niobium, or hydrogen in tantalum. In addition, for a certain range of ratios, our isotherms share some of the features of the isotherms found experimentally when argon is adsorbed on graphitized carbon black.[6]

In Sec. II we review the properties of the superexchange model that were found by Fisher. We also make a comparison between the phase boundaries of the superexchange model and the phase boundaries of the Ising antiferromagnet. In Sec. III we describe the method used to obtain the equation of state. The results are discussed and the phase diagrams for different values of the ratio of the antiferromagnetic to ferromagnetic coupling are given. In Sec. IV we discuss the interpretation of our model both as a decorated lattice-gas model and as a host-impurity system.

II. REVIEW OF PROPERTIES OF SUPEREXCHANGE MODEL AND COMPARISON WITH ISING ANTIFERROMAGNET

A. Superexchange model

The superexchange antiferromagnet[3] is a standard two-dimensional square Ising lattice which has been decorated by placing a magnetic spin on each bond. At each vertex of the Ising lattice there is a nonmagnetic spin. By nonmagnetic we mean that the spin interacts with only infinitesimal coupling with the magnetic field, i.e., its magnetic moment is zero. The interactions are between the nonmagnetic vertex spins and the magnetic bond spins. The signs of the interactions are positive (ferromagnetic) on vertical bonds and negative (antiferromagnetic) on horizontal bonds as shown in Fig. 1. This ensures that the magnetic spins, which lie on a square lattice at an angle of 45° with respect to the original lattice, will be antiferromagnetically ordered in the ground state. The model captures many of the features of those real antiferromagnetic materials in which the coupling takes place indirectly via a nonmagnetic intermediary atom,[7] although it lacks some of the details of the superexchange interaction found in such materials.

If we denote $s_i = \pm 1$ as the spin variable of a nonmagnetic or vertex spin, $s_j = \pm 1$ as the spin variable of a magnetic spin on a vertical bond, and $s_k = \pm 1$ as the spin variable of a magnetic spin on a horizontal bond, then the Hamiltonian is

$$\mathcal{H}_{SE} = -J_{SR} \sum_{vb} s_i s_j + J_{SR} \sum_{hb} s_i s_k - \mu H_0 \sum_{j=1}^{N} s_j - \mu H_0 \sum_{k=1}^{N} s_k, \tag{2.1}$$

where H_0 is the applied magnetic field, J_{SR} is the strength of the nearest-neighbor (short-range) interaction, μ is the magnetic moment of the magnetic spins, N is the number of vertex, vertical, or horizontal spins (so that there are $3N$ spins all together), and $\sum_{vb}$ ($\sum_{hb}$) is the sum over all vertical (horizontal) bonds. If we introduce the dimensionless parameters

$$K = J_{SR}/kT, \quad L = \mu H_0/kT, \quad \alpha = \mu H_0/2J_{SR}, \tag{2.2}$$

where T is the temperature and k is Boltzmann's constant, we may write the partition function as

$$Z(K,L) = \sum_{s_i=\pm 1} \sum_{s_j=\pm 1} \sum_{s_k=\pm 1} \times \exp\left(K \sum_{vb} s_i s_j - K \sum_{hb} s_i s_k + L \sum_{j=1}^{N} s_j + L \sum_{k=1}^{N} s_k\right). \tag{2.3}$$

By introducing a modified interaction parameter $G(K,L)$, Fisher[3] is able to obtain the following form for the partition function, $Z(K,L)$, of the decorated lattice:

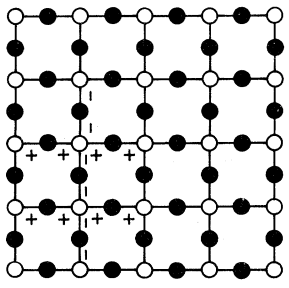

FIG. 1. The superexchange antiferromagnet.

$$Z(K,L)=[f(K,L)]^{2N}\sum \exp G(K,L)\,s_i\,s_j$$

$$=[f(K,L)]^{2N}Q(G(K,L)). \tag{2.4}$$

Here $Q(G)$ is the partition function of the standard square Ising lattice of N spins in zero field with nearest-neighbor interaction energy $J^*=kTG$. The functions $f(K,L)$ and $G(K,L)$ are defined by the equations

$$f^4(K,L)=2^4\cosh(2K+L)\cosh(2K-L)\cosh^2 L, \tag{2.5}$$

$$e^{4G(K,L)}=\cosh(2K+L)\cosh(2K-L)/\cosh^2 L. \tag{2.6}$$

The decoration transformation[8] [Eqs. (4)–(6)] is a mapping of the antiferromagnetic decorated lattice at temperature T ($\sim 1/K$) and magnetic field H ($\sim L$) onto the standard Ising lattice in zero field at modified temperature T^* ($\sim 1/\mathrm{kG}$). The thermodynamics of the decorated lattice can be derived in terms of Onsager's solution[9] for the standard square Ising lattice in zero field and the model can therefore be solved exactly.

The equation of state for the magnetic spins in this model can be obtained in the usual manner. The reduced magnetization per vertex is defined as

$$M(K,L)=\frac{I}{\mu N}=N^{-1}\left(\frac{\partial \ln Z(K,L)}{\partial L}\right)_K, \tag{2.7}$$

where I is the total magnetization of the lattice (which is just the sum of the magnetizations of the spins on the vertical and horizontal bonds). The saturation value of the magnetization is given by $M_s=2$. The magnetization can be obtained by using Eqs. (4)–(7) in conjunction with Onsager's solution. This yields

$$M(K,L)=\left(\frac{\partial G}{\partial L}\right)_K U^*(G)+2\left(\frac{\partial \ln f}{\partial L}\right)_K, \tag{2.8}$$

where

$$U^*(G)=\{1+[2\tanh^2(2G)-1](2/\pi)K(k_1)\}\coth(2G) \tag{2.9}$$

is the reduced energy of the standard square net as defined by Onsager and

$$k_1=2\tanh 2G/\cosh 2G \tag{2.10}$$

is the modulus of the complete elliptic integral of the first kind. Thus, the equation of state, $M(K,L)$, can be represented by a surface in M, T, H_0 space. For its projections onto the M-T, M-H_0, and H_0-T planes see Figs. 9, 10, and 11 of Fisher (Ref. 3). The transition field as a function of temperature, $H_t(T)$, is shown in Fisher's Fig. 11 by the dashed line. Below this transition curve, long-range antiferromagnetic order prevails with magnetic spins on vertical and horizontal bonds pointing predominantly in opposite directions. Above the transition curve the behavior is essentially paramagnetic.

The susceptibility of the magnetic spins can also be determined

$$\chi=\frac{\partial M(K,L)}{\partial H_0}=\frac{\mu^2}{kT}\left(\frac{\partial^2 \ln Z(K,L)}{\partial L^2}\right)_K$$

$$=\mu^2(kT)^{-1}\left[\left(\frac{\partial^2 G}{\partial L^2}\right)_K U^*(G)+\left(\frac{\partial G}{\partial L}\right)_K^2 D^*(G)+2\left(\frac{\partial^2 \ln f}{\partial L^2}\right)_K\right], \tag{2.11}$$

where $D^*(G)$ is simply related to the specific heat C^* of the standard square Ising net. More explicitly

$$D^*(G)=\frac{\partial^2 \ln Q(G)}{\partial G^2}=\frac{\partial U^*}{\partial G}=\frac{kT^{*2}C^*}{J_{SR}^2}$$

$$=2\coth^2 2G\left(\frac{2}{\pi}K(k_1)-\frac{2}{\pi}E(k_1)-\frac{1}{2}(1-k_1'')\left[1+k_1''\frac{2}{\pi}K(k_1)\right]\right), \tag{2.12}$$

where $E(k_1)$ is the complete elliptic integral of the second kind with modulus k_1 and

$$k_1''=2\tanh^2(2G)-1. \tag{2.13}$$

The initial (or zero-field) susceptibility is a continuous and smoothly varying function of T with a maximum 40% above the critical point, however $\partial\chi/\partial T$ is infinite at $T=T_c=1.30841/k$. For $H_0\neq 0$, the susceptibility has a logarithmic singularity as a function of temperature at the transition point $T=T_t(H_0)$.

Since we can calculate the susceptibility as a function of temperature and field and the magnetization as a function of temperature and field, we can graph the inverse susceptibility versus the magnetization for fixed values of the temperature. In Fig. 2 we plot $(J_{SR}\chi_{SP})^{-1}$ versus M for different values of the reduced temperature K^{-1}. Notice the spike to zero in the inverse susceptibility which is an indication that at that particular temperature and magnetization a phase transition will take place. As the temperature is increased from zero the spike moves from $M_t=0.58579$ at $T=0$ towards the $M=0$ axis until at $T=T_c=1.30841$ (J_{SR}/k) the spike is absorbed into the $M=0$ axis. Above this temperature there is no spike present, and hence there is no phase transition. Notice that as T approaches T_c from below a hump is developing in the inverse susceptibility [see

$T=1.25$ (J_{SR}/k) as an example]. At the saturation value of the magnetization (not shown) the inverse susceptibility goes to infinity. This graph will be of importance to us when we try to survey qualitatively the effects of adding a long-range ferromagnetic interaction to the superexchange antiferromagnet.

B. Comparison with Ising-model results

It is of interest to compare the H-M-T surface of the superexchange antiferromagnet with results for the standard nearest-neighbor Ising antiferromagnet, some of which were unavailable to Fisher at the time he introduced the superexchange model. Plischke and Mattis[10] and others[11] have presented the solution to the nearest-neighbor Ising antiferromagnet using molecular field theory (MFT). We wish to point out that just as the MFT treatment of a ferromagnetic interaction is equivalent to the exact treatment of an infinitely weak and infinitely long-range ferromagnetic interaction potential, the MFT treatment of an antiferromagnetic interaction is equivalent to the exact treatment of an infinitely weak and infinitely long-range staggered interaction. This important conclusion has not to our knowledge been explicitly stated previously in the literature, although closely related results have been given by Høye[12] and by Gates[13] and the validity of the general result follows as a direct extension of their work.

A comparison of the phase diagrams of the superexchange model and the phase diagrams found by Plischke and Mattis in their MFT treatment of the nearest-neighbor Ising model shows that in MFT, the phase transition at $T=0$ occurs at $M=M_s$, whereas in the superexchange model the transition occurs at $M=0.70441M_s$. Also, in MFT the transition field has a maximum at a nonzero temperature whereas in the superexchange model the maximum occurs at $T=0$.

We may also compare the superexchange results with two sets of "exact" nearest-neighbor Ising-model results. Plischke and Mattis[10] have used the transfer-matrix method to look at an Ising antiferromagnet on an $M\times N$ square lattice where $N=\infty$ and $M=8$. Bienenstock[14] has used an expansion technique to study both two- and three-dimensional antiferromagnetic Ising lattices. The superexchange antiferromagnet has a phase diagram which is very similar to the two-dimensional diagrams of both Plischke and Mattis and of Bienenstock.

The results of our comparison in two dimensions strongly suggest the following general conclusion: The exact nearest-neighbor Ising model results and the superexchange model results are more similar to each other than either is to the results of the mean-field approximation to the Ising model.

III. ADDITION OF AN EQUIVALENT-NEIGHBOR FERROMAGNETIC INTERACTION TO THE SUPEREXCHANGE ANTIFERROMAGNET

In this section we discuss the changes that result in the equation of state when a weak, long-range ferromagnetic interaction is added to the potential of the superexchange antiferromagnet. The discussion can be given in terms of either the equivalent-neighbor ferromagnetic interaction[1] or the Kac potential.[2] Here we shall use the equivalent-neighbor language for the sake of convenience.

The Hamiltonian for the system now under consideration is given by

$$\mathcal{H}=\mathcal{H}_{SE}+\mathcal{H}_{LR},$$

$$\mathcal{H}=-J_{SR}\sum_{vb}s_i s_j+J_{SR}\sum_{hb}s_i s_k-H\sum_{j=1}^{N}s_j - H\sum_{k=1}^{N}s_k-\frac{J_{LR}}{2N}\sum_{l=1}^{2N}\sum_{l'=1}^{2N}s_l s_{l'}, \tag{3.1}$$

where $\mathcal{H}_{SE}$ is the Hamiltonian for the superexchange antiferromagnet and J_{LR} is the strength of the long-range interaction. The quantity

$$\mathcal{H}_{LR}=-\frac{J_{LR}}{2N}\sum_{l=1}^{2N}\sum_{l'=1}^{2N}s_l s_{l'} \tag{3.2}$$

is the equivalent-neighbor potential which is a very weak and long-range ferromagnetic interaction that becomes infinitely weak and infinitely

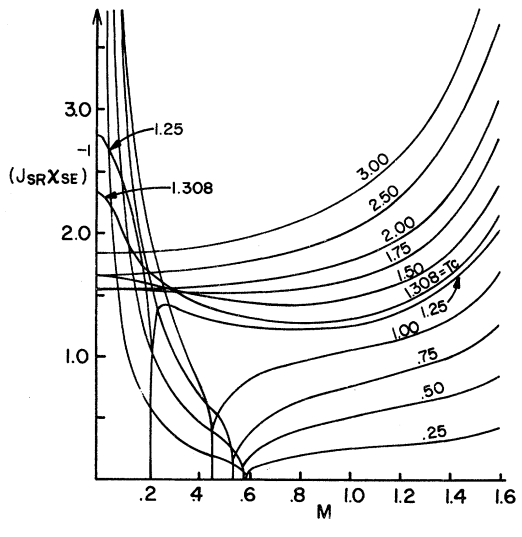

FIG. 2. Inverse susceptibility as a function of magnetization for fixed temperature. The curves are labeled by the appropriate value of the reduced temperature K^{-1}.

long range in the thermodynamic limit. The sum is over all the magnetic spins. It can be shown[1] that the equation of state for this system, $H(M, T)$, can be expressed in terms of the equation of state of the superexchange model, $H_0(M, T)$, by the following transformation:

$$H(M, T) = [H_0(M, T) - 2J_{LR}M] + \text{Maxwell type of construction.} \quad (3.3)$$

A graph of field H versus the magnetization M for fixed J_{LR} and T will have van der Waals loops. A necessary condition for equilibrium is that the Gibbs free energy per spin, $F(H, T)$,[15] of the two phases be equal. Differences between $F(H, T)$ on any point on the curve and some reference point are given by

$$F(H, T) - F_{ref} = -\int_{H_{ref}}^{H} M dH = -\int_{\alpha_{ref}}^{\alpha} M(1 - 2J_{LR}\chi_{SE})2J_{SR}d\alpha, \quad (3.4)$$

where the integration variable α is defined in Eq. (2.2). The Maxwell type of construction referred to in Eq. (3.3) is just an equal-area construction in the H-M plane. For computational purposes we prefer to find the magnetizations at the transition point by locating the intersection point on a graph of $[F(H, T) - F_{ref}]$ vs H where $H_{ref} = 0$.

It can be shown that Eq. (3.3) also holds for the case of a three-dimensional metamagnet in which spins in the same plane interact via a superexchange antiferromagnetic interaction while spins in different planes interact via a ferromagnetic equivalent-neighbor interaction. We find that if we define the magnetization variable to be $\sum_{i=1}^{2N^2} s_i/N^2$, where N equals the number of planes as well as the number of vertices, the equations are identical to the equations found for the two-dimensional superexchange antiferromagnet with equivalent-neighbor interactions. Thus, the results which we have obtained also describe the behavior of this three-dimensional metamagnet.

A. Qualitative behavior of the equation of state – Spinodal line

We find that much useful qualitative information as well as some exact quantitative information can be obtained from an inspection of graphs of simple thermodynamic functions of the reference system.[16] In particular, we shall consider graphs of the susceptibility versus the magnetization for the reference system, as shown in Fig. 2. The susceptibility of the full system can be expressed in terms of the susceptibility of the reference system by differentiating Eq. (3.3). Thus

$$\frac{1}{\chi} = \left(\frac{dH}{dM}\right)_T = \frac{2J_{SR}d\alpha}{dM} - 2J_{LR} = \frac{1}{\chi_{SE}} - 2J_{LR} \quad (3.5)$$

or

$$\frac{1}{J_{SR}\chi} = \frac{1}{J_{SR}\chi_{SE}} - \frac{2J_{LR}}{J_{SR}}.$$

When $(dH/dM)_T = 1/\chi = 0$, which occurs when $1/\chi_{SE} = 2J_{LR}$, we get a spinodal point which is just the maximum or minimum point of the van der Waals loops. Since the transition magnetizations will bracket the spinodal point magnetizations, the location of the spinodal points gives us a good indication of where the transition magnetizations will lie. The critical point is a special spinodal point at which not only $1/\chi = 0$ but also $d(1/\chi)/dM = 0$. In order to find the spinodal points for a particular value of the ratio J_{LR}/J_{SR} and temperature T we locate on Fig. 2 the intersection points of the curve $1/J_{SR}\chi_{SE}$ and the constant $2J_{LR}/J_{SR}$. To find the critical point we locate the tangency point between the curve $1/J_{SR}\chi_{SE}$ and the constant $2J_{LR}/J_{SR}$.

As an example of how to obtain qualitative and quantitative information about the full system from the reference system graph of $1/J_{SR}\chi_{SE}$ vs M, we will focus our attention on particular temperature values (which are scaled by the short-range interaction strength). For the following discussion refer to Fig. 2. For $kT/J_{SR} = 1$ there are two spinodal points for $0 < 2J_{LR}/J_{SR} < \infty$. This means that at $kT/J_{SR} = 1$ there will always be a first-order phase transition about some value M ($M \neq 0$). For $kT/J_{SR} = 1.5$, there are no spinodal points for $2J_{LR}/J_{SR} < 1.415$, there is a critical point for $2J_{LR}/J_{SR} = 1.415$, there are two spinodal points for $1.67 > 2J_{LR}/J_{SR} > 1.415$, and there is one spinodal point for $2J_{LR}/J_{SR} > 1.67$. This means that at $kT/J_{SR} = 1.5$ there will be no phase transition for $J_{LR}/J_{SR} < 1.415$, a critical point for $2J_{LR}/J_{SR} = 1.415$, a first-order transition about $M \neq 0$ for $1.67 > 2J_{LR}/J_{SR} > 1.415$, and a first-order transition about $M = 0$ for $2J_{LR}/J_{SR} > 1.67$. In this manner we can determine qualitatively the behavior of the full system for each value of J_{LR}/J_{SR} and kT/J_{SR}.

B. Phase boundaries

We now describe the phase boundaries which have been calculated for different values of the ratio J_{LR}/J_{SR}. Throughout this section we shall loosely refer to the temperature variable as "T" and to the field variable as "H." Actually the temperature variable is the reduced temperature kT/J_{SR} and the field variable is the reduced field H/J_{SR}. We have divided the range of values of the ratio J_{LR}/J_{SR} into different regions. Within each region

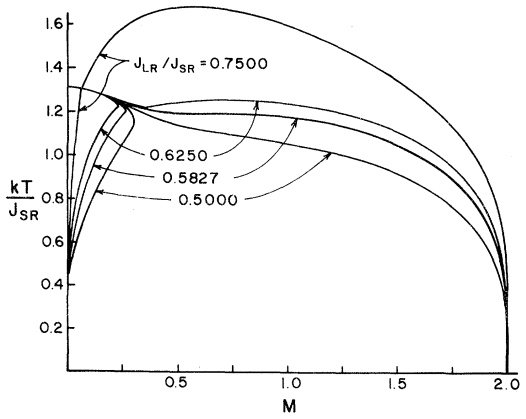

FIG. 3. Phase boundary in the T-M plane for J_{LR}/J_{SR} = 0.500 (region I), 0.5827 (region II), 0.625 (region II), and 0.750 (region III).

the transitional behavior is qualitatively the same for different values of the ratio. For each region we pick a typical value for the ratio and show the exact phase boundaries in H-T space and in T-M space. Finally we present a diagram in the kT/J_{SR} vs J_{LR}/J_{SR} plane which delineates the different regions and shows more fully the behavior which occurs. All of these calculations were performed on the IBM 360 computer at the State University of New York at Stony Brook.

a. Region I: $0 \leq J_{LR}/J_{SR} < 0.5827$. We choose as a typical value for this region $J_{LR}/J_{SR} = 0.5$. For $T > (T_c)_{SE}$ (the critical temperature of the superexchange antiferromagnet), there are no phase transitions. At $T = (T_c)_{SE}$, a critical point at $M = 0$, $H = 0$ develops. As T decreases below $(T_c)_{SE}$, the critical point separates into two first-order phase transitions about nonzero values of M and at nonzero values of H. The transition near $T = (T_c)_{SE}$ is always of first order. At $T = 0$ it can be shown by a simple geometric argument that the value of H at the phase boundary for any value of J_{LR}/J_{SR} is given by $H(T = 0) = 2 - 2J_{LR}/J_{SR}$ and the values of M at the phase boundary are $M = 0$ and $M = \pm 2$. The M-T phase boundary for $J_{LR}/J_{SR} = 0.500$ is shown in Fig. 3 and the H-T phase boundary is shown in Fig. 4. Note that although the M-T diagrams are symmetric about $M = 0$, we will only show the right-half plane. Similarly, in the H-T diagrams we will show only the upper-half plane. In the region between the $M = 0$ axis and the left-hand side of the phase boundary we find antiferromagnetic behavior. The area above and to the right of the phase boundary is paramagnetic.

b. Region II: $0.5827 \leq J_{LR}/J_{SR} < 0.655$. For $T > (T_c)_{SE}$ there are no phase transitions. At $T = (T_c)_{SE}$ a critical point at $M = 0$, $H = 0$ develops. As T decreases below $(T_c)_{SE}$, this critical point separates into two first-order phase transitions centered at a nonzero value of M and at a nonzero value of H. At $T = T_c$ a second critical point develops at some nonzero field and magnetization. For $T < T_c$ there are four phase transitions until at $T = T_{TP}$ (the triple-point temperature) they merge into two phase transitions. At $T = 0$ the phase transitions have boundary points at $M = 0$, $M = \pm 2$ and at $H = 2 - 2J_{LR}/J_{SR}$.

The M-T and H-T phase boundaries for $J_{LR}/J_{SR} = 0.5827$ and 0.625 are shown in Figs. 3, 4, and 5. We have included the value $J_{LR}/J_{SR} = 0.5827$ which is the left-hand endpoint of this region because it is at this value that the second critical point first appears. The value $J_{LR}/J_{SR} = 0.5827$ may be characterized as the point at which $T_{TP} = T_c$ or as the point at which $d^2(1/J_{SR}\chi)/dM^2 = d^2(1/J_{SR}\chi_{SE})/dM^2 = 0$.

The region to the left of the phase boundary in M-T space is antiferromagnetic and the region

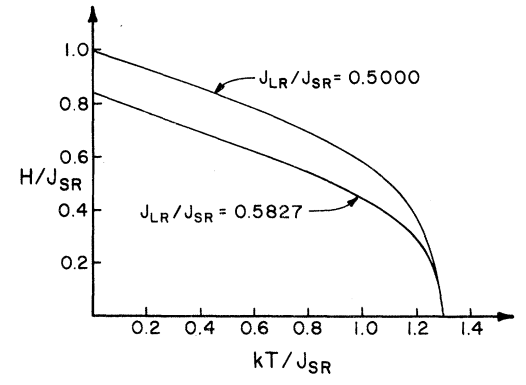

FIG. 4. Phase boundary in the H-T plane for J_{LR}/J_{SR} = 0.500 (region I) and $J_{LR}/J_{SR} = 0.5827$ (region II).

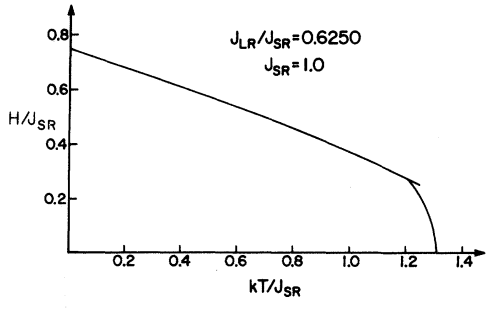

FIG. 5. Phase boundary in the H-T plane for J_{LR}/J_{SR} = 0.625 (region II).

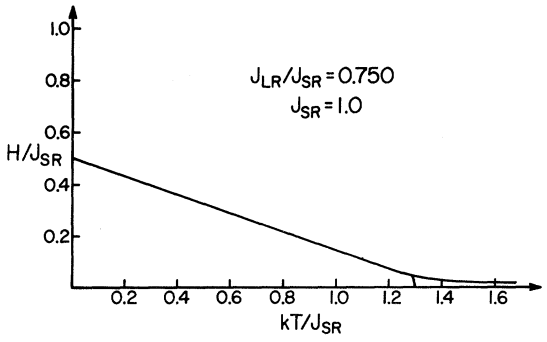

FIG. 6. Phase boundary in the H-T plane for $J_{LR}/J_{SR} = 0.750$ (region III).

above and to the right is paramagnetic.

c. Region III: $0.655 \leq J_{LR}/J_{SR} < 0.7667$. The behavior in this region is very similar to that described for region II. The only difference is that here $T_c > (T_c)_{SE}$ whereas in region II, $T_c < (T_c)_{SE}$. The M-T and H-T phase boundaries for $J_{LR}/J_{SR} = 0.750$ are shown in Figs. 3 and 6. The region to the left of the phase boundary in M-T space is antiferromagnetic and the region above and to the right of the phase boundary is paramagnetic.

d. Region IV: $0.7667 \leq J_{LR}/J_{SR} < 0.7770$. This is a very small region. We have chosen as a typical value for this region $J_{LR}/J_{SR} = 0.7700$. For $T > T_c$ there are no phase transitions. At $T = T_c$ a critical point develops at $M = \pm M_c$, $H = \pm H_c$. As T decreases below T_c the critical point spreads into two first-order phase transitions centered at some nonzero value of M until at $T = T_{TP}^{(1)}$ the phase transitions merge to become one transition about $M = 0$ and at $H = 0$. At $T = T_{TP}^{(2)} < T_{TP}^{(1)}$ the transition breaks into two transitions and moves to $|H| > 0$. At $T = (T_c)_{SE}$ a second critical point develops at $M = 0$, $H = 0$. For $T < (T_c)_{SE}$ there are four phase transitions and for $T = T_{TP}$ there is a triple point at which these four transitions merge into two transitions. At $T = 0$ there are two transitions with boundaries $M = 0$ and $M = \pm 2$ and transition field $H = 2 - 2J_{LR}/J_{SR}$. The left-hand endpoint of this region, $J_{LR}/J_{SR} = 0.7667$, is the point at which $T_{TP}^{(1)} = T_{TP}^{(2)} = 1.58$. The right-hand endpoint of this region, $J_{LR}/J_{SR} = 0.7770$, is the point at which $T_{TP}^{(2)}$, $(T_c)_{SE}$, and T_{TP} all meet at $M = 0$. It is also the point at which $T_{TP}^{(1)} = T_c$ at $M = 0$. The phase boundaries in the M-T and H-T plane for $J_{LR}/J_{SR} = 0.7700$ are shown in Figs. 7 and 8. In the M-T plane the area between the $M = 0$ axis and the left-hand side of the phase boundary below $T = (T_c)_{SE}$ is an antiferromagnetic region. The area directly above this is a paramagnetic region. The area to the right of the phase boundary is paramagnetic.

e. Region V: $0.7770 \leq J_{LR}/J_{SR} < 1.000$. We choose as a typical value of J_{LR}/J_{SR} in this region the value $J_{LR}/J_{SR} = 0.875$. For $T > T_c$ there are no phase transitions. At $T = T_c$ a critical point develops at $M = 0$, $H = 0$. At $T = T_{TP}^{(2)}$ this phase transition splits into two smaller transitions centered at nonzero M and at nonzero H. At $T = 0$ the phase transitions have boundary points at $M = 0$, $M = \pm 2$ and at $H = 2 - 2J_{LR}/J_{SR}$. The right-hand endpoint of this region, $J_{LR}/J_{SR} = 1$, is the point at which $T_{TP}^{(2)} = 0$, i.e., for $J_{LR}/J_{SR} = 1$, $H = 0$ at $T = 0$. The phase boundaries in M-T space and H-T space for $J_{LR}/J_{SR} = 0.875$ are shown in Figs. 9 and 10. The area to the left of the phase boundary is antiferromagnetic, and the area above and to the right of the phase boundary is paramagnetic.

f. Region VI: $J_{LR}/J_{SR} \geq 1.000$. The qualitative

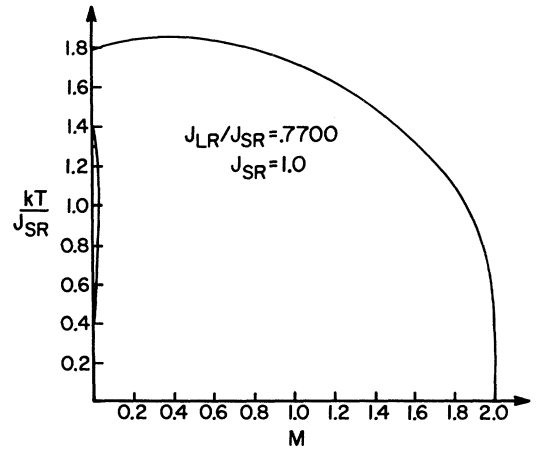

FIG. 7. Phase boundary in the T-M plane for $J_{LR}/J_{SR} = 0.770$ (region IV).

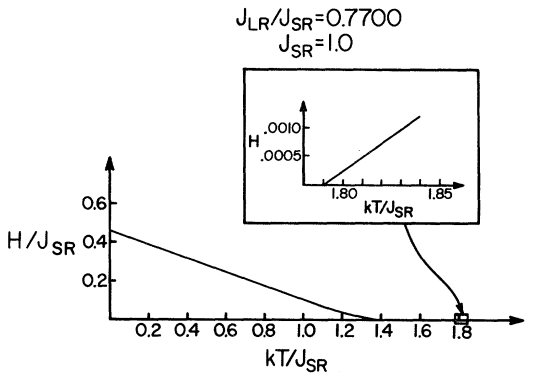

FIG. 8. Phase boundary in the H-T plane for $J_{LR}/J_{SR} = 0.770$ (region IV).

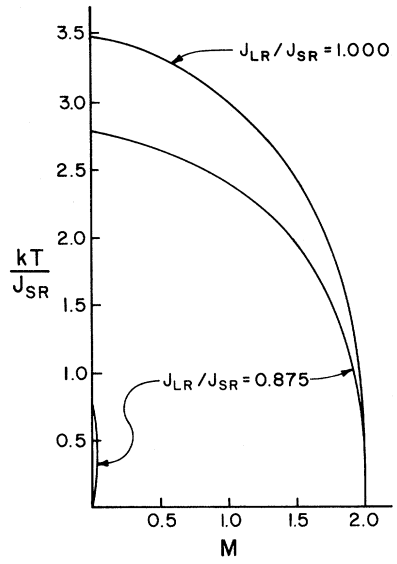

FIG. 9. Phase boundary in the T-M plane for $J_{LR}/J_{SR} = 0.875$ (region V) and $J_{LR}/J_{SR} = 1.000$ (region VI).

behavior throughout this region is similar to the behavior at its endpoint, $J_{LR}/J_{SR} = 1$. For $T > T_c$ there are no phase transitions, at $T = T_c$ a critical point develops at $M = 0$, $H = 0$, and for $T < T_c$ there is one phase transition centered at $M = 0$ and at $H = 0$. The phase boundaries in the M-T and H-T planes are shown in Figs. 9 and 11. We see that as the strength of the long-range interactions becomes greater than the strength of the short-range interaction, we obtain a diagram in M-T space that looks qualitatively like the coexistence curve of a simple lattice gas with infinitely weak and infinitely long-range attractions. The area to the right of the phase boundary is paramagnetic.

Thus we have seen how the addition of an infinitely weak and infinitely long-range ferromagnetic interaction to the potential of the superexchange antiferromagnet changes the phase behavior of that system. Where once there were only single second-order phase transitions there are now first-order phase transitions with rather complicated structures that change as J_{LR}/J_{SR} is varied.

Figure 12 summarizes the behavior that we have described in this section. In the $kT/J_{SR} - J_{LR}/J_{SR}$ plane we show the boundary lines $T = (T_c)_{SE}$, $T = T_c$, $T = T_{TP}$, $T = T_{TP}^{(1)}$ and $T = T_{TP}^{(2)}$. The number of phase transitions within each area is also indicated.

IV. OTHER SYSTEMS DESCRIBED BY THE SAME DECORATED-LATTICE MODEL

A. Lattice-gas interpretations of the results

In order to more fully understand the significance of our results we shall interpret them in terms of fluid or lattice-gas language in this section. It has long been known that there is a close analogy[18] between the thermodynamic behavior of magnetic systems described by the variables M, H and T, and the behavior of systems such as a one-component fluid that are described by the variables P, v, and T where P is the pressure, v is the specific volume ($v = 1/\rho$) and T is the temperature. This analogy has been very much illuminated by the Yang-Lee[19] demonstration of the isomorphism between the Ising model and the lattice gas, an extension of which we give in the next section. The analogy was well known prior to that demonstration and can be understood from a purely thermodynamic viewpoint, divorced from the details of a particular pair of isomorphic models. There are in fact two well-known alternative thermodynamic correspondences between P, v, T and M, H, T systems. The first is given by the correspondence (up to additive and multiplicative constants)

$$p \leftrightarrow H,$$
$$v \leftrightarrow -M, \tag{4.1}$$

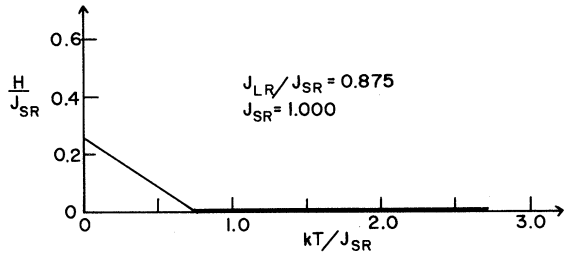

FIG. 10. Phase boundary in the H-T plane for $J_{LR}/J_{SR} = 0.875$ (region V).

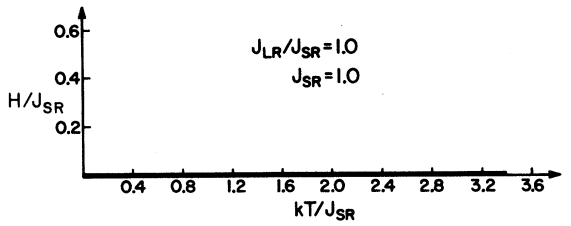

FIG. 11. Phase boundary in the H-T plane for $J_{LR}/J_{SR} = 1.000$ (region VI).

while the second is given most directly in terms of the chemical potential μ (again up to additive and multiplicative constants)

$$\mu \rightarrow H, \qquad \rho \rightarrow M. \tag{4.2}$$

The second correspondence is also yielded by the usual Ising-model–lattice-gas isomorphism. There are two routes to a lattice-gas interpretation of our model both of which yield Eq. (4.2). The first involves an extension of a lattice-gas version of the superexchange antiferromagnet that was first proposed by Fisher. The second involves an interpretation based upon a direct superexchange-model–decorated-lattice-gas isomorphism that is an extension of the Ising-model–lattice-gas isomorphism of Yang and Lee.

1. *Correspondence with Fisher's planar lattice gas*

Fisher[17] considered a square lattice gas with nearest-neighbor repulsions of strength V_1 and next-nearest-neighbor attractions across alternate squares of the lattice. The model can be solved exactly for the case $V_1 \rightarrow \infty$ (i.e., when it becomes a hard-core lattice gas), but only for one particular isotherm. In order to so solve it, Fisher first considered the general case in which the hard core is softened, i.e., $V_1 \neq \infty$. He also introduced one other interaction, a "four-body" repulsive interaction of strength $V^* = 4GkT$ which comes into play between adjacent atoms when the remaining two sites in the alternate squares are unoccupied. This interaction was introduced as a device which enabled him to transform the problem into the superexchange model.

It is a simple matter to find how his results change when an infinitely weak and infinitely long-range attractive interaction of strength ϵ_{LR}/N (which is the lattice-gas version of the equivalent-neighbor potential) is added to the potential of the soft-core lattice gas. It can be shown, however, that for a given set of interaction parameters, the behavior of this soft-core lattice gas with long-range attractions can be found for only a single isotherm. For this reason we cannot relate the phase boundaries of this lattice gas to the phase boundaries of our model. Therefore we have not considered this model any further.

2. *Superexchange-antiferromagnet-decorated lattice-gas isomorphism*

A second way to make an identification between the superexchange antiferromagnet with equivalent-neighbor ferromagnetic interactions and a lattice gas with infinitely weak and infinitely long-range attractions is to make a direct Ising-model–to–lattice-gas transformation. In this section we describe the results of this transformation and show how to interpret our spin-system phase boundaries in lattice-gas terms.

In order to make the correspondence with lattice-gas language we let $s_l = +1$ (where $l = i, j, k$) correspond to an occupied site and $s_l = -1$ correspond to an unoccupied site. If we designate τ_l as the occupation variable so that $\tau_l = 1$ indicates an occupied state and $\tau_l = 0$ indicates an unoccupied state then $s_l = 2\tau_l - 1$. Substituting this into the Hamiltonian [Eq. (3.1)] and proceeding in the usual manner[19] we find that the partition function of the superexchange antiferromagnet with weak long-range attractions is related to the grand partition function of a lattice gas with infinitely weak and infinitely long-range attractions in the following way:

$$Z(K, L, J_{LR}/kT) = e^{-2NL+2NJ_{LR}}\,\Xi(z_i, z_j, z_k, \epsilon_{SR}/kT, \epsilon_{LR}/kT)$$

or

$$e^{-F/kT} = e^{-2NL+2NJ_{LR}}\,e^{3NP/kT}, \tag{4.3}$$

where now

$$\begin{aligned} z_i &= 1, \\ z_j &= 2(L - 2K - 2J_{LR}/N), \\ z_k &= 2(L + 2K - 2J_{LR}/N), \\ 4J_{SR} &= \epsilon_{SR}, \\ 4J_{LR} &= \epsilon_{LR}. \end{aligned} \tag{4.4}$$

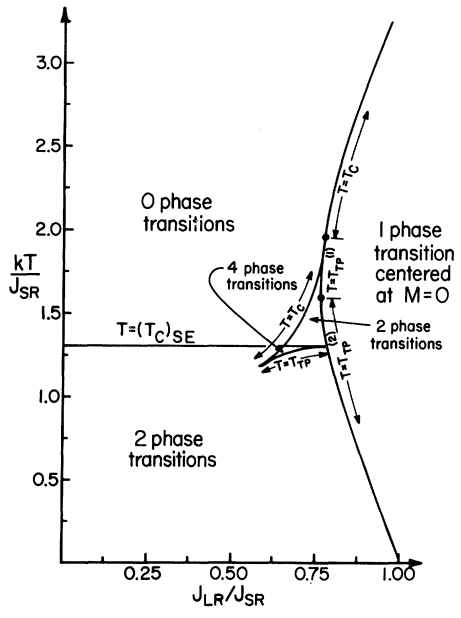

FIG. 12. Diagram in the kT-J_{LR}/J_{SR} plane showing the boundary lines $T = (T_c)_{SE}$, $T = T_{TP}$, $T = T_{TP}^{(1)}$ and $T = T_{TP}^{(2)}$. The number of phase transitions within each area is also indicated.

The magnetization that was given in Eq. (2.8) corresponds to a density function, ρ, of the j and k particles:

$$\rho = \tfrac{1}{2}(\rho_j + \rho_k) = \tfrac{1}{4}(M+2), \tag{4.5}$$

where $\rho_j = \sum \tau_j/N$ and $\rho_k = \sum \tau_k/N$. The magnetization of the vertex or i particles, J^0, which was calculated by Fisher corresponds to the denstiy of the i particles, ρ_i. In order to find the density of the i particles by the formula $\rho_i = z_i(\partial/\partial z_i)(\ln\Xi)$, a limiting process must be taken since z_i = constant. This yields

$$\rho_i = \tfrac{1}{2}(J^0+1). \tag{4.6}$$

Thus we have found a decorated lattice gas with infinitely weak and infinitely long-range attractions that is isomorphic to the model that we have been studying. The interactions are the same, i.e., a particle on a vertical bond site will be attracted to its nearest neighbors and a particle on a horizontal site will be repelled by its nearest neighbors.

From Eq. (4.3) the pressure-field relationship for this decorated-lattice-gas model is

$$P = \tfrac{2}{3}H - \tfrac{2}{3}J_{\mathrm{LR}} - (\text{free energy})/\text{spin}. \tag{4.7}$$

Alternatively, we may wish to find the pressure in terms of the variables M and H. To do this we make use of the following relation:

$$dP = s\,dT + \rho_i\,d\mu_i + \rho_j\,d\mu_j + \rho_k\,d\mu_k. \tag{4.8}$$

Then the pressure is given by

$$P(\mu) - P(\mu=-\infty) = \int_{-\infty}^{\mu_i} \rho_i\,d\tilde{\mu}_i + \int_{-\infty}^{\mu_j} \rho_j\,d\tilde{\mu}_j + \int_{-\infty}^{\mu_i} \rho_k\,d\tilde{\mu}_k, \tag{4.9}$$

where T is constant. Now $d\tilde{\mu}_i = 0$ (since μ_i is a constant), $P(\mu=-\infty)=0$ and $d\mu_j = d\mu_k$ at constant T so that

$$P = \int_{-\infty}^{H} \tfrac{1}{2}(M+2)\,d\tilde{H}. \tag{4.10}$$

In this way we are able to relate the thermodynamics and hence the phase diagrams of our model to the equivalent thermodynamics of a P,V,T model. The phase boundaries in M-T space will map into a coexistence curve in ρ-T space via Eq. (4.5) since lines of singularities in one space are mapped into lines of singularities in the other space.

In Figs. 13–16 we present the coexistence curves in P-ρ space and the phase diagrams in P-T space for $\epsilon_{\mathrm{LR}}/\epsilon_{\mathrm{SR}} = J_{\mathrm{LR}}/J_{\mathrm{SR}} = 0.500$, 0.625, 0.750, 0.875, and 1.000. (We have not included any diagram for region IV.) The coexistence curve in ρ-T space can easily be visualized because it is the same as the full M-T diagram. The curves in the P-ρ plane (in which there is frequent crossing of isotherms), are rather unusual and warrant some comments.

First we notice that the P-T curves in Figs. 13 and 14 have a temperature maximum at $T = (T_c)_{\mathrm{SE}}$ as a function of pressure. For example, see the curve for $\epsilon_{\mathrm{LR}}/\epsilon_{\mathrm{SR}} = 0.500$ in Fig. 13. The lower part of this curve is for $\rho < \frac{1}{2}$ and the upper part is for $\rho > \frac{1}{2}$. The reasons for the occurrence of this feature become clear when we recall that the pressure corresponding to a certain field, H, is an area in the H-M plane as described in Eq. (4.10). For $H<0$ ($M<0$ or $\rho<\frac{1}{2}$) this area increases with increasing temperature and for $H>0$ ($M>0$ or $\rho>\frac{1}{2}$) this area decreases with increasing temperature. The unusual shape in the P-ρ plane for $\rho>\frac{1}{2}$ (it looks "upside down") reflects the fact that the pressure decreases with increasing temperature. The coexistence curve on the $\rho>\frac{1}{2}$ side is inverted about the pressure at which the temperature is a maximum. In fact, we can say that any magnetic Ising system which is symmetric about $M=0$, has a nonzero transition field, H, such that $H>0$ for $M>0$ and $H<0$ for $M<0$, and such that the absolute value of H decreases with increasing temperature, will have a temperature maximum as a function of pressure in its corresponding lattice-gas system. This temperature maximum as a function of pres-

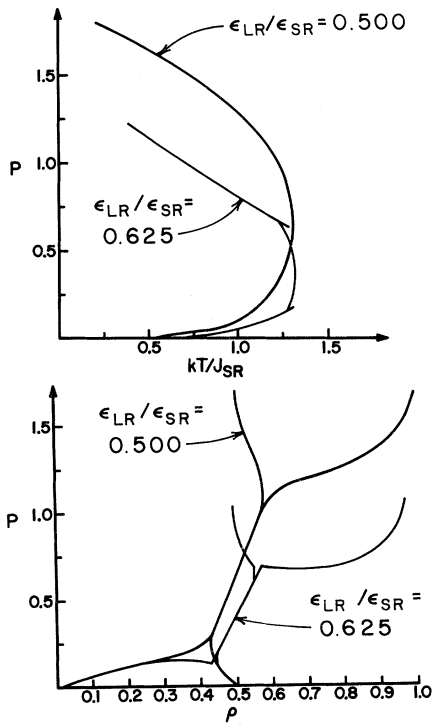

FIG. 13. Coexistence curve and phase boundary for $\epsilon_{\mathrm{LR}}/\epsilon_{\mathrm{SR}} = 0.500$ and for $\epsilon_{\mathrm{LR}}/\epsilon_{\mathrm{SR}} = 0.625$.

sure was also noted by Matsuda,[20] in his study of the three-dimensional lattice gas with repulsive nearest neighbors using the mean-field approximation. The melting temperature maximum as a function of pressure has been observed in many solids.[21] Usually, in association with this maximum, the solid also exhibits a solid-solid transition at some higher pressure. This does not happen in our model nor does it happen in Matsuda's approximation.

In Fig. 13 we also present the coexistence curve and phase diagram for $\epsilon_{LR}/\epsilon_{SR}=0.625$. The critical point has already appeared as the endpoint of a spur in the P-T plane and at the top of the usual dome in the P-ρ plane for $\rho<\frac{1}{2}$. It is accompanied by its inverted image in the P-ρ plane for $\rho>\frac{1}{2}$.

For $\epsilon_{LR}/\epsilon_{SR}=0.750$ (see Fig. 14) the spur and its image in the P-T plane have lengthened. The pressure of the upper spur first decreases and then increases as a function of temperature. This change in direction is reflected in the P-ρ plane for $\rho>\frac{1}{2}$ by another inversion in the already inverted coexistence curve.

For $\epsilon_{LR}/\epsilon_{SR}=0.875$ (see Fig. 15) the behavior is markedly different. For $T<T_{TP}^{(2)}$ the P-T curve has the characteristic temperature maximum feature at $T=T_{TP}^{(2)}$. For $T>T_{TP}^{(2)}$ there is just one curve in which the pressure increases with temperature. (Recall that for $T>T_{TP}^{(2)}$ there is one extended transition about $M=0$.) The coexistence curve in P-ρ space is relatively complicated and difficult to represent in two dimensions. The best way to understand it is to trace out the isotherms. For $T<T_{TP}^{(2)}$ the isotherms resemble step functions with origin at $\rho=\frac{1}{2}$. For $T>T_{TP}^{(2)}$, the isotherms have a more familiar behavior which ends in a critical point.

For $\epsilon_{LR}/\epsilon_{SR}=1.0$ (see Fig. 16) the behavior is most familiar. The effects of the long-range interactions have increased to the point where we have a coexistence curve whose shape qualitatively resembles that of a lattice gas with simple hard cores and attractive interactions.

B. Interpretation of model as a host-impurity problem

The decorated lattice gas discussed in the last section lends itself to immediate interpretation as a host-impurity system. We define the host particles as those particles that are located on the vertices of the lattice and the impurity particles as those particles that are located on the bond sites. The presence of a host particle can be thought of as corresponding to a spin-up on a vertex and the presence of an impurity particle to a spin-up on a bond site. Spin-down indicates that

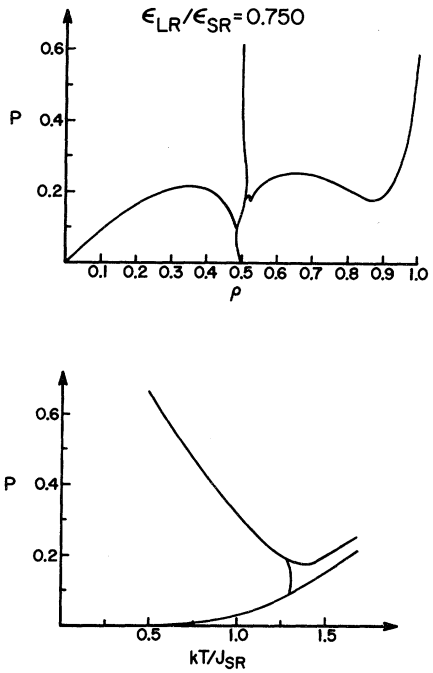

FIG. 14. Coexistence curve and phase boundary for $\epsilon_{LR}/\epsilon_{SR}=0.750$

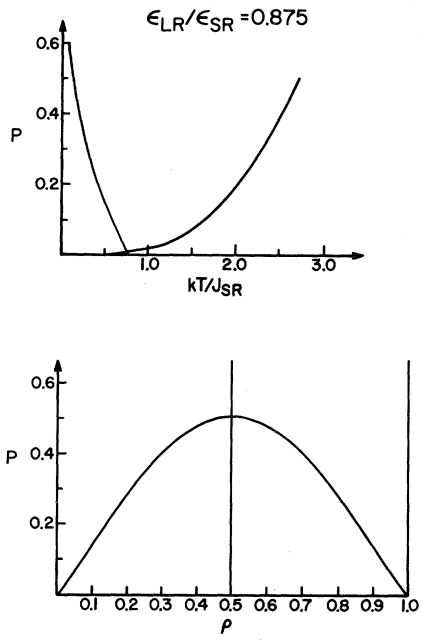

FIG. 15. Coexistence curve and phase boundary for $\epsilon_{LR}/\epsilon_{SR}=0.875$.

the site is unoccupied. Thus, looking at the problem presented in the last section in slightly different language we have

$$\rho_{\text{imp}} = \tfrac{1}{2}(\rho_j + \rho_k) = \tfrac{1}{4}(M+2), \tag{4.11}$$

$$\rho_{\text{host}} = \rho_i . \tag{4.12}$$

Alternatively we can imagine that *all* vertex sites are occupied by host particles, but that only some of them become activated by the impurities. Then spin-up on a vertex corresponds to an *activated* host particle and spin-down to an inactive host particle that is not interacting with impurities. Under this mapping the ρ_{host} of (4.12) corresponds to the density of activated host sites. It is this interpretation of ρ_{host} that seems most relevant to host-impurity problems of physical interest. Both the interaction energy between the impurity and the host and the chemical potential of the impurity are determined by which of the two sites (horizontal or vertical) the impurity particle occupies. For certain values of the variables one of the sites will be preferentially occupied. This corresponds to antiferromagnetic ordering in the equivalent magnetic system. For other values (when the equivalent magnetic system is in a paramagnetic state) the sites will be occupied with equal probability.

We now discuss a family of host-impurity systems whose thermodynamic behavior is similar to the thermodynamic behavior found in our model. Hydrogen-metal systems such as hydrogen in niobium, in tantalum, and in palladium have been of growing interest to physicists in recent years. One of the problems that remains unsolved is that of deriving theoretically the phase diagrams that occur for these systems. It has been known for many years[22] that the hydrogen-palladium system is amenable to study by a simple nearest-neighbor lattice-gas approach. This particular system has a coexistence curve with a critical point that resembles a typical van der Waals type coexistence curve. The other systems are not as well understood theoretically since the phase diagrams are more complicated.

The phase diagrams for H in Ta,[23] Nb,[24] and Pd,[25] are shown schematically in Figs. 17(a), 17(b), and 17(c), respectively, as they are usually plotted in the $T-x$ plane where $x=\rho_{\text{imp}}/\rho_{\text{host}}$. Since $\rho_{\text{host}} \approx 1$ for hydrogen-metal systems, we can think of these diagrams as being essentially $T-\rho_{\text{imp}}$ phase diagrams and hence compare them with the $T-\rho_{\text{imp}}$ phase diagrams of our model. We see that the phase boundaries in $T-\rho_{\text{imp}}$ space for $\epsilon_{\text{LR}}/\epsilon_{\text{SR}}=0.5827$, 0.675, and 1.000 as shown in Figs. 17(d), 17(e), and 17(f) reproduce qualitatively the coexistence curves of H in Ta, Nb, and Pd, respectively. In addition to this similarity between the shapes of the coexistence curves in our model and the shapes of the coexistence curves in hydrogen-metal systems there is a correspondence between the phases in our model and the phases in hydrogen-metal systems.

We begin by discussing the hydrogen-niobium system which is the most general of the three hydrogen-metal systems that we will consider. The hydrogen atoms occupy interstitial sites within the niobium's bcc lattice structure.[26]

In the hydrogen-niobium phase diagram there are three phases α, α', and β phases. The α and α' phases are regions of low and high hydrogen concentrations, respectively. These two phases, which can coexist as regions of compression and dilitation, differ in that the lattice parameter of the α phase is smaller than the lattice parameter of the α' phase. Both the α and α' phases retain the cubic symmetry of the niobium lattice so that all of the interstitial sites will be occupied with equal probability. In the β phase the lattice becomes orthorhombic and looses the cubic symmetry of the niobium lattice. This occurs because certain of the available impurity sites are preferentially occupied by hydrogen atoms, thus distorting the host lattice.

Now let us compare the phase diagrams that we have found in regions II and III ($0.5827 < \epsilon_{\text{LR}}/\epsilon_{\text{SR}} < 0.7667$) with the phase diagram of the hydrogen-

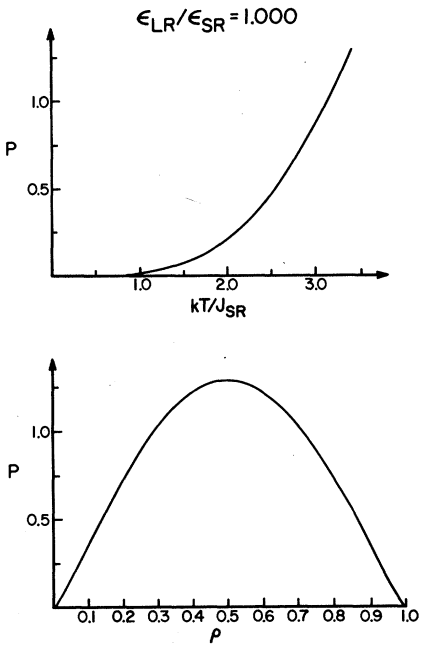

FIG. 16. Coexistence curve and phase boundary for $\epsilon_{\text{LR}}/\epsilon_{\text{SR}} = 1.000$.

niobium system [Fig. 17(b)]. In Fig. 17(e) we have plotted the phase diagram for $\epsilon_{LR}/\epsilon_{SR}=0.675$ which has typical behavior for this region. In our model there is a coexistence region between two phases, one of low impurity concentration and the other of high impurity concentration. In both of these phases, the two sites available to the impurity atoms are occupied with equal probability. We can identify these two phases with the α and α' phases of the H-Nb system. There is a third phase of very high impurity concentration in which one of the two sites available to the impurity atom is preferentially occupied. We can identify this phase with the β phase of the H-Nb system.

We can make similar identifications between the phase diagrams found in the H-Ta and H-Pd systems and the phase diagrams of our model shown in Figs. 17(d) and 17(f). In the H-Ta phase diagram the triple point temperature just equals the critical point temperature so that the α' phase that was present in the H-Nb system no longer appears. In our model this occurs when the parameter $\epsilon_{LR}/\epsilon_{SR}=0.5827$. In this case we have a coexistence region between a phase of low impurity concentration in which the two sites available to the impurity atoms are occupied with equal probability and a phase of high impurity concentration in which one of the two sites available to impurity atoms is preferentially occupied. These phases can be identified with the α and β phases of the H-Ta system.

In the H-Pd phase diagram there is a coexistence region between the α and α' phases. Once again it is possible to identify these phases with the two phases in our model present when $\epsilon_{LR}/\epsilon_{SR} \geq 1$.

Thus we see that the shapes of the coexistence curves of hydrogen-metal systems are qualitatively similar to the shapes of the coexistence curves in our model and that it is possible to make a direct identification between the α and α', and β phases of hydrogen-metal systems and the phases found in our model.

There are several ways in which our model appears to capture certain key features of hydrogen-metal systems. In particular, they are the following: (i) The model contains two different species which can be viewed as host and impurity particles. These two species reside on separate lattices so that the impurity particles are interstitial rather than substitutional. There are two distinguishable impurity sites per host atom. (ii) The model contains a very-long-range attractive interaction between the impurity atoms. It has been suggested[5,27] that there is indeed a long-range attractive interaction between hydrogen atoms dissolved in metals and that this may be due to elastic forces.[28] (iii) The model contains a mechanism for the creation of preferential occupation of sites which appear to be a necessary feature if one is to obtain the β phase.

On the other hand, our model contains certain features which do not seem to correspond in any obvious way to the physics of hydrogen-metal systems. For instance, we can think of no reason why hydrogen-metal systems should literally have attractive interactions on bonds between hydrogen and metal atoms in certain directions and repulsive interactions on bonds between hydrogen and metal atoms in other directions. The possible relevance of this type of interaction for hydrogen-metal system is rather that is serves as a mechanism for obtaining impurity ordering, i.e., preferential occupation of certain sites. A second obvious difference is in dimensionality. However, since the qualitative behavior of Ising models is well known to be the same in two and three dimensions, the *qualitative* nature of our results should be independent of dimensionality. At the same time, there is little sense in our making a quantitative comparison between the two-dimensional version of our model studied here and experimental metal-hydrogen results, and we have not attempted such a comparison.

Such differences notwithstanding, we think it is significant that in a single model we have been able to obtain phase diagrams which have shapes similar to the shapes of the experimentally observed H-Nb, H-Ta, or H-Pd phase diagrams and

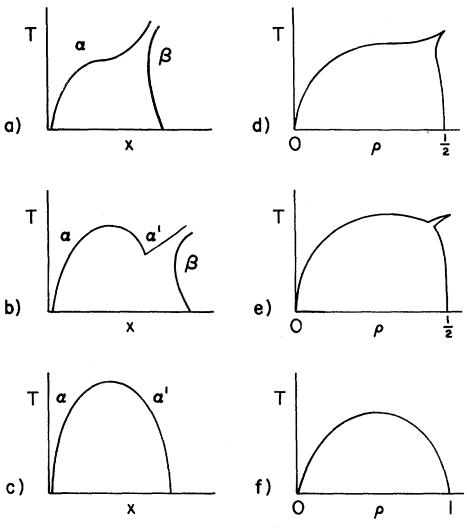

FIG. 17. Diagram showing schematic drawings of the phase boundaries in the temperature-concentration plane for (a) tantalum, (b) niobium, and (c) palladium. For comparison we have presented the coexistence curves of our model in the temperature-density plane for $\epsilon_{LR}/\epsilon_{SR}$ = (d) 0.5827, (e) 0.675, and (f) 1.000.

have phases which can be directly related to the α, α', and β phases that are found in these hydrogen-metal systems. We hope that this may provide a new viewpoint for modeling the physics of hydrogen-metal systems.

It is also of interest to compare our results to the results for real two-dimensional host-impurity systems such as adsorption systems. In region II, typified by $\epsilon_{LR}/\epsilon_{SR} = 0.625$, the phase diagrams for $\rho < \frac{1}{2}$ are in agreement with what is known of the experimental phase diagrams for argon adsorbed on a substrate of graphitized carbon black. However, the available experimental results are too sparse to allow comparison for more than a few isotherms.[6] Our model may prove to be of even greater value as a model of chemisorption than of such physical adsorption. At the very least, because of the great similarity between the properties of the two-dimensional superexchange antiferromagnet and the two-dimensional Ising antiferromagnets, our model should be useful in studies of chemisorption for the same reasons that the Ising model with nearest-neighbor repulsion and longer range attraction has already been found useful.[29] Our model has the immense added advantage that it is exactly solvable. But more than that, its built-in host-impurity structure may make it and its immediate generalizations[30] more natural than the Ising model in this connection, and it automatically incorporates many of the features to which other workers have already been led from quite different starting points.[31] For example, the indirect superexchange interaction between adatoms via activated host sites can be taken as the "through-bond" interaction discussed in Ref. 31 and references therein, while the longer-range direct adatom-adatom interaction can be taken as the "through-space" interaction of that reference.

In closing, we note that although our model shares many of the features common to most systems with competing interactions, there is one striking difference: the lack of a tricritical point of the sort found experimentally in He^3-He^4 mixtures and expected[32] in the Ising model with nearest-neighbor antiferromagnetic interactions and next-nearest-neighbor ferromagnetic interactions. In order for such a tricritical point to be found in our model, the sharp spike which goes down to the horizontal axis in Fig. 2 would have to terminate at some nonzero value of χ^{-1}. We conjecture that a graph of χ^{-1} vs M for the Ising antiferromagnet may differ from our Fig. 2 in just this respect, so that if we were using the Ising antiferromagnet instead of the superexchange antiferromagnet as a reference system, we would expect to find a tricritical point of the He^3-He^4 type at $M \neq 0$ over a certain range of values of J_{LR}/J_{SR}.

Our model *does* exhibit another type of tricritical point of the type found in Nagle's one-dimensional Ising chain[1] with nearest-neighbor antiferromagnetic interactions and equivalent-neighbor ferromagnetic interactions.[33] In fact we find that our model exhibits all of the complexity found in the Nagle model (including its version of a tricritical point) in the subregion of our Fig. 17 defined by $T > (T_c)_{SE}$.

ACKNOWLEDGMENTS

We are grateful to Jill Bonner for suggesting the use of the superexchange model as a reference system and to John Nagle for helpful comments.

---

*Work supported by the National Science Foundation under Grant No. GP-21311.

†This work constitutes a portion of a thesis submitted by Carol K. Hall to the faculty of the State University of New York at Stony Brook in partial fulfillment of the requirements for the Ph.D. degree.

‡Present address (to which reprint requests should be sent): Dept. of Chemistry, Cornell University, Ithaca, N.Y. 14853.

[1]G. A. Baker, Jr., Phys. Rev. 130, 1406 (1963) and references therein; J. F. Nagle, Phys. Rev. A 2, 2124 (1970).

[2]The use of the Kac potential for lattice systems has been discussed in detail by M. Kac and E. Helfand, J. Math. Phys. 4, 1078 (1963). For general arguments applicable to lattice and fluid systems see J. Lebowitz and O. Penrose, J. Math. Phys. 7, 98 (1966). See also C. J. Thompson, *Mathematical Statistical Mechanics* (MacMillan, New York, 1972).

[3]M. E. Fisher, Proc. R. Soc. A 254, 66 (1960); A256, 502 (1960).

[4]One of the key results of Refs. 1 and 2 is that the Weiss-Bragg-Williams approximation (mean-field theory) becomes correct for infinite range of interaction.

[5]G. Alefeld, Phys. Status Solidi 32, 67 (1969); G. Alefeld in *Critical Phenomena in Alloys, Magnets and Superconductors,* edited by R. E. Mills *et al*. (McGraw-Hill, New York, 1971), p. 339; G. Alefeld, Ber. Gunsenges, Phys. Chem. 76, 355 (1972).

[6]C. F. Prenzlow and C. D. Halsey, J. Phys. Chem. 61, 1158 (1957).

[7]We refer here to the superexchange coupling described by P. W. Anderson, Phys. Rev. 79, 350 (1950). Note that the coupling in the Fisher superexchange model is similar in spirit but not in detail to the more realistic superexchange coupling mechanism described by Anderson.

[8]For a general description of the decoration transformation see M. E. Fisher, Phys. Rev. 113, 969 (1959).

[9]L. Onsager, Phys. Rev. 65, 117 (1944).
[10]M. Plischke and D. Mattis, Phys. Rev. A 3, 2092 (1971).
[11]C. G. B. Garrett, J. Chem. Phys. 19, 1154 (1951).
[12]J. S. Høye, Phys. Rev. B 6, 4261 (1972), and unpublished.
[13]D. J. Gates (private communication).
[14]A. Bienenstock, J. Appl. Phys. 37, 1459 (1966).
[15]Here we use the notation and conventions of T. L. Hill [*Statistical Mechanics* (McGraw-Hill, New York, 1956), Chap. 7.]
[16]C. K. Hall and G. Stell, Phys. Rev. A 7, 1679 (1973).
[17]M. E. Fisher, J. Math. Phys. 4, 278 (1963).
[18]See for example, H. B. Callen, *Thermodynamics* (Wiley, New York, 1966).
[19]T. D. Lee and C. N. Yang, Phys. Rev. 87, 410 (1952).
[20]H. Matsuda, Prog. Theor. Phys. 42, 140 (1969).
[21]See references cited in Ref. 20.
[22]J. R. Lacher, Proc. R. Soc. 161, 525 (1937).
[23]Schematic drawing of hydrogen in palladium taken from Ref. 5. See for example D. P. Smith, *Hydrogen in Metals* (University of Chicago Press, Chicago, 1948); H. Brodowsky and E. Peoschel, Z. Phys. Chem. Neuefolge 44, 143 (1965).
[24]Schematic drawing taken from Ref. 5 based on the work of H. Zierath, thesis (Universitat Munster, 1969) (unpublished).
[25]Schematic drawing based on work by R. J. Walter and W. T. Chandler, Trans. AIME 233, 762 (1965).
[26]M. O'Keefe and S. A. Steward, Proceedings of the International Meeting on Hydrogen in Metals, Kernforschungsanlage, Julich, Germany, March 1972 (unpublished).
[27](a) H. Buck and G. Alefeld, Phys. Status Solidi B 47, 193 (1971). (b) H. Wagner and H. Horner (unpublished).
[28]For a discussion of other possible reasons for the attractive interaction see Sec. 3.3 of Ref. 27(b).
[29]T. L. Einstein and J. R. Schrieffer, Phys. Rev. B 7, 3629 (1973). See end of Sec. III.
[30]Some of these generalizations have been explored by one of us in G. Stell, SUNY College of Engineering Report No. 241 (1973), available upon request.
[31]T. B. Grimley and M. Torrini, J. Phys. C 6, 868 (1973).
[32]The Ising model with first- and second-neighbor interactions has been studied by C. J. Gortor and Tineke Van-Peski Tinbergen using mean-field theory. See Physica 22, 273 (1956). More recent work on this model using Monte Carlo techniques has been reported by D. Landau, Phys. Rev. Lett. 28, 449 (1972) and series-extrapolation results are given by F. Harbus and H. E. Stanley, Phys. Rev. B 8, 1156 (1973).
[33]For a precise description of this type of tricritical point see J. C. Bonner and J. F. Nagle, J. Appl. Phys. 42, 1280 (1971).